Raman and infrared spectra, conformational stability, normal coordinate analysis and ab initio calculations of 3-chloro-1-butene

ARTICLE *in* JOURNAL OF RAMAN SPECTROSCOPY · MARCH 2000

Impact Factor: 2.67 · DOI: 10.1002/(SICI)1097-4555(200003)31:3<157::AID-JRS513>3.0.CO;2-2

JOURNAL OF RAMAN SPECTROSCOPY
J. Raman Spectrosc. **31**, 157–169 (2000)

Raman and infrared spectra, conformational stability, normal coordinate analysis and *ab initio* calculations of 3-chloro-1-butene

Min Joo Lee,[1] Feng Fusheng,[2] Seung Won Hur,[3]† Jian Liu,[3]‡ Todor K. Gounev[3] and James R. Durig[3]*

[1] Department of Chemistry, Changwon National University, Changwon, Kyungnam 641-773, Republic of Korea
[2] Measuring and Testing Center, Taiyuan University of Technology, Taiyuan, Shanxi 030024, China
[3] Department of Chemistry, University of Missouri–Kansas City, Kansas City, Missouri 64110-2499, USA

The Raman and infrared spectra (3300–30 cm^{-1}) of gaseous and solid 3-chloro-1-butene, $H_2C{=}CHCCl(CH_3)H$, were recorded. Additionally, the Raman spectrum (3300–30 cm^{-1}) of the liquid was recorded. All three conformers were observed in the flui phases and the conformer with the hydrogen atom eclipsing the double bond (HE form) was identifie as the most predominant. From variable-temperature measurements in liquifie xenon, the enthalpy differences between the HE form and the two less stable conformers, i.e. the methyl group eclipsing the double bond (ME form) and the chlorine atom eclipsing the double bond (ClE form), were determined to be 75 ± 8 cm^{-1} (214 ± 23 cal mol^{-1}) and 197 ± 37 cm^{-1} (563 ± 106 cal mol^{-1}), respectively. Nearly complete vibrational assignments are proposed for all three conformers, which are consistent with the predicted wavenumbers utilizing the force constants from *ab initio* MP2/6–31G(d) calculations. Both the infrared intensities and the Raman activities and depolarization values were obtained from the *ab initio* calculations. Complete equilibrium geometries were determined by *ab initio* calculations employing the 6–31G(d) and 6–311++G(d,p) basis sets with full electron correlation by the Möller–Plesset (MP2) perturbation method to second order. The structural parameters obtained with the larger basis set are comparable to those obtained from a previously reported electron diffraction study. The results are discussed and the theoretical values are compared with the experimental values when appropriate.

INTRODUCTION

The 3-chloro-1-butene molecule has received considerable attention with regard to its conformation.[1–4] In previous vibrational spectroscopic investigations,[1,2] it was concluded that at least two conformers coexist at ambient temperature; however, these two studies disagreed on the stability of the conformers. From a gas-phase electron diffraction study[3] of this molecule it was determined that the conformer with the hydrogen atom eclipsing the double bond (HE; Fig. 1) has 76 ± 10 and $62 \pm 10\%$ population at 20 and 180 °C, respectively, with some contribution from the conformer with the chlorine atom eclipsing the double bond (ClE). Although these investigators[1–3] did not exclude the possibility of a third conformer, there was no conclusive evidence for it.

In theoretical studies,[3,4] the conformer with the methyl group eclipsing the double bond (ME) and the ClE conformation were calculated to have only 1.0–1.3 kcal mol^{-1} (350 to 455 cm^{-1}) higher energy than the HE form. With such an energy difference, the two high-energy conformers (ME and ClE) should be present in detectable amounts at ambient temperature. Therefore, in order to investigate the presence of the third conformer and to determine the conformational stabilities and the enthalpy differences, we carried out Raman and infrared spectral studies of the gas, liquid and annealed solid. Additionally, we carried out variable-temperature infrared spectral studies in xenon solutions to obtain the enthalpy differences among the conformers. *Ab initio* calculations using the 6–31G(d) and 6–311++G(d,p) basis sets at the level of restricted Hartree–Fock (RHF) and/or with full electron correlation by the perturbation method to second order (MP2) were also carried out to predict the conformational stability, energy differences, structural parameters, Raman and infrared intensities and vibrational wavenumbers.

EXPERIMENTAL

The sample of 3-chloro-1-butene was obtained from Aldrich Chemical (Milwaukee, WI, USA). Purificatio was carried out by using a low-temperature, low-pressure

* Correspondence to: J. R. Durig, Department of Chemistry, University of Missouri–Kansas City, Kansas City, Missouri 64110-2499, USA; e-mail: durigj@umkc.edu
† Taken in part from the dissertation of S. W. Hur, which will be submitted to the Department of Chemistry in partial fulfillmen of the PhD degree.
‡ Present address: Watson Pharmaceuticals, Inc., 132A Business Center Dr., Corona, CA 97120, USA.
Contract/grant sponsor: University of Missouri–Kansas City Faculty Research Grant Program.

Received 4 July 1999
Accepted 3 September 1999

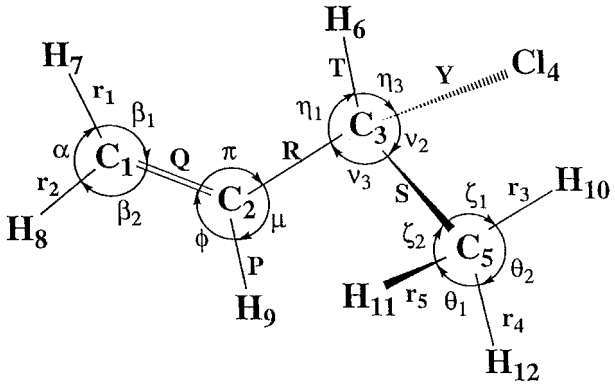

Figure 1. Internal coordinates for the HE conformer of 3-chloro-1-butene.

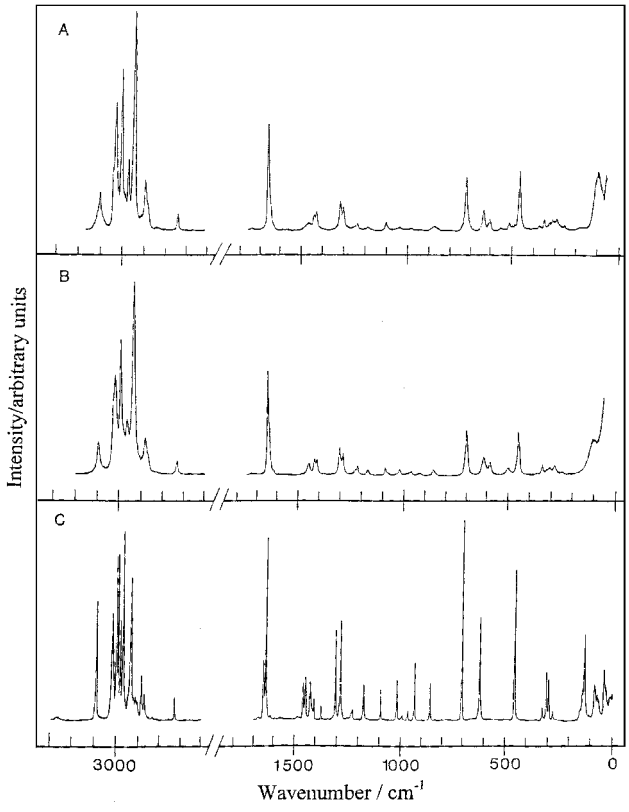

Figure 2. Raman spectra of 3-chloro-1-butene in the (A) gas, (B) liquid and (C) annealed solid.

fractionation column and the sample was stored under vacuum in a slush of ethanol and dry ice.

The Raman spectra (Fig. 2) were recorded on a Cary Model 82 spectrophotometer equipped with a Spectra-Physics Model 171 argon ion laser with excitation of 514.5 nm radiation. The Raman spectrum of the gas was recorded by using a standard Cary multipass accessory. Reported wavenumbers are expected to be accurate to at least ± 2 cm^{-1}. The spectrum of the liquid was obtained from the sample sealed in a Pyrex capillary. The spectrum of the annealed solid was recorded by using a Model DTC-500 cryogenic temperature controller (Lake Shore Cryogenics).

The mid-infrared spectra of the gaseous and annealed solid (Fig. 3) were recorded on a Digilab Model FTS-14C Fourier transform interferometer equipped with a Ge/KBr beamsplitter and a TGS detector. For the gaseous sample,

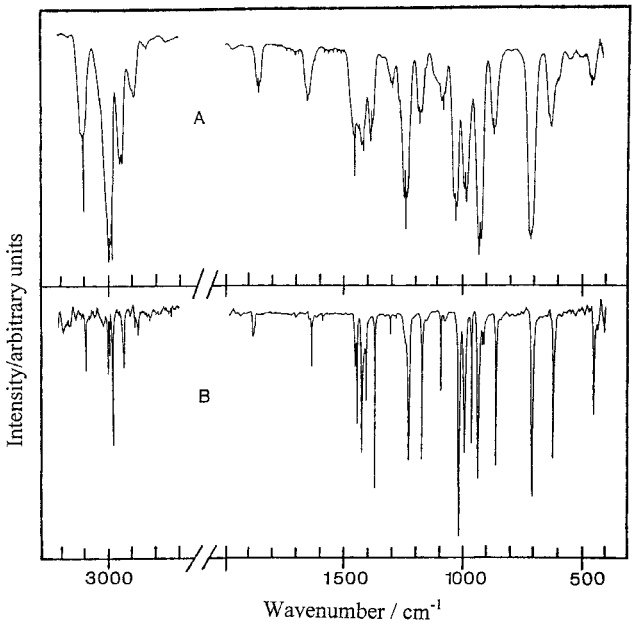

Figure 3. Mid-infrared spectra of 3-chloro-1-butene in the (A) gas and (B) annealed solid.

a 10 cm cell fitte with CsI windows was employed. The spectrum of the annealed solid was obtained by depositing the sample on a CsI plate cooled by boiling liquid nitrogen and housed in a cell fitte with CsI windows.

The far-infrared spectra (Fig. 4) were recorded on a Perkin-Elmer Model 2000 Fourier transform interferometer equipped with a ceramic source, a grid beamsplitter and a DTGS detector. For the gaseous sample, a 10 cm cell fitte with polyethylene windows was employed. The sample was dried with calcium hydride. A cryostat cell with polyethylene windows and an Si substrate was used for the solid sample, and the sample was maintained at $-196\,^{\circ}$C by boiling liquid nitrogen.

The mid-infrared spectra of the sample dissolved in liquifie xenon as a function of temperature [Fig. 5(A)] were recorded on a Bruker Model IFS-66 Fourier transform interferometer equipped with a globar source, a Ge/KBr beamsplitter and a DTGS detector. The temperature studies ranged from -55 to $-100\,^{\circ}$C and were performed in a specially designed cryostat cell consisting of a 4 cm pathlength copper cell with wedged silicon windows sealed to the cell with indium gaskets. The complete system is attached to a pressure manifold to allow for the fillin and evacuation of the cell. The cell is cooled by boiling liquid nitrogen and the temperature is monitored by two Pt thermoresistors. Once the cell is cooled to the desired temperature, a small amount of sample is condensed into the cell. The system is then pressurized with xenon gas, which immediately starts to condense, allowing the compound to dissolve. For each temperature investigated, 100 interferograms were recorded at 1.0 cm^{-1} resolution, averaged and transformed with a boxcar truncation function. All of the observed infrared and Raman bands are listed in Table 1.

AB INITIO CALCULATIONS

LCAO–MO–SCF restricted Hartree–Fock calculations were performed with the Gaussian-94 program[5] using

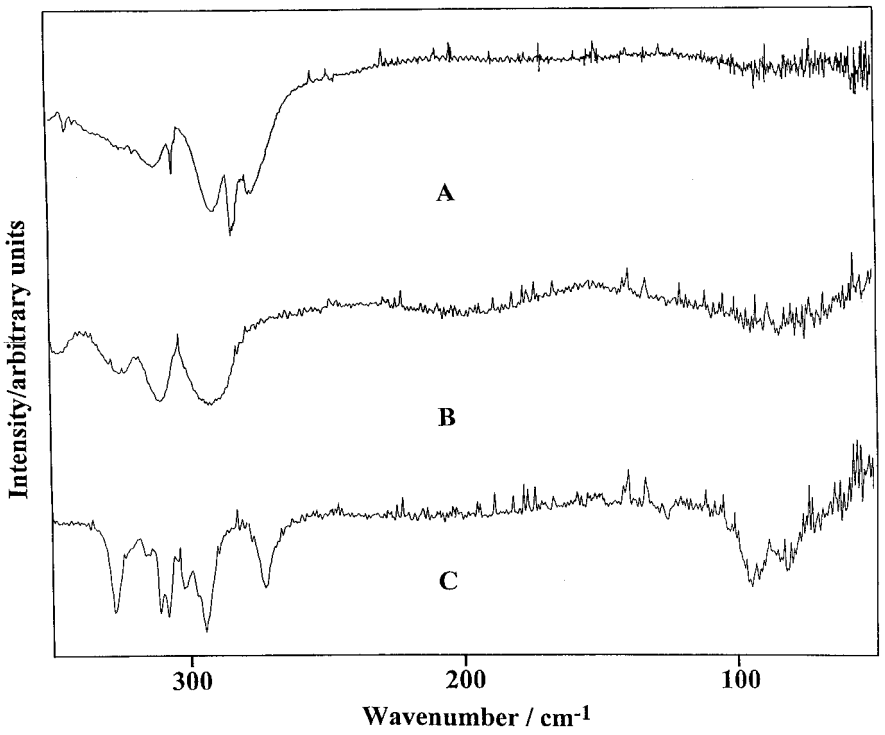

Figure 4. Far-infrared spectra of 3-chloro-1-butene in the (A) gas, (B) unannealed solid and (C) annealed solid.

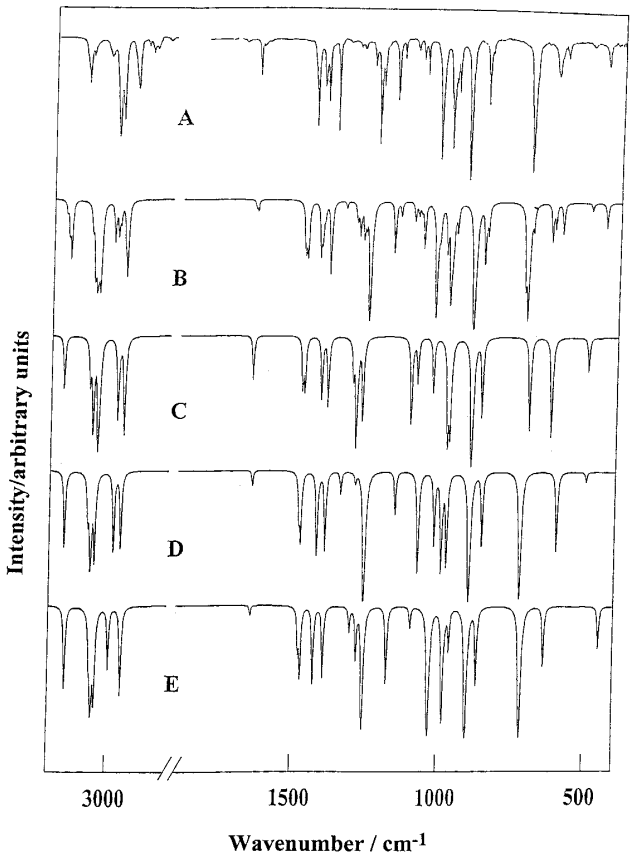

Figure 5. Mid-infrared spectra of 3-chloro-1-butene: (A) xenon solution at −85 °C; (B) calculated spectrum of the mixture of all three conformers; (C) calculated spectrum of the CIE conformer; (D) calculated spectrum of the ME conformer; (E) calculated spectrum of the HE conformer.

Gaussian-type basis functions. The energy minima with respect to the nuclear coordinates were obtained by the simultaneous relaxation of all of the geometric parameters using the gradient method of Pulay.[6] The 6–31G* and 6–311++G** basis sets were employed at the level of restricted Hartree–Fock (RHF) and/or Möller–Plesset (MP2) to second order[7] with full electron correlation. The predicted structural parameters are listed in Table 2.

The energies of the potential minima and maxima during internal rotation along the =C—C bond were obtained by the simultaneous relaxation of all of the structural parameters using the MP2/6–31G* basis set. The resulting values of the energies were fi to an asymmetric potential function of the type

$$V(\phi) = \sum_{i=1}^{6}(V_i/2)(1 - \cos i\phi) + \sum_{i=1}^{5}(V_i'/2)\sin i\phi$$

where ϕ is the torsional dihedral angle. The resulting potential function is shown in Fig. 6 with the values of the potential coefficient and the barriers to internal rotation listed in Table 3.

In order to obtain a more complete description of the molecular motions involved in the normal modes of 3-chloro-1-butene we carried out a normal coordinate analysis. This analysis was performed utilizing *ab initio* calculations and the Wilson matrix method.[8] The force fiel in Cartesian coordinates was calculated by the Gaussian-94 program with the MP2/6–31G* basis set. The Cartesian coordinates obtained for the optimized structure were input into the *G*-matrix program[9] together with a complete set of 34 internal coordinates (Fig. 1). This complete set of internal coordinates was used to form the symmetry coordinates (Table 4). The output of the *G*-matrix program gives the *B*-matrix which was used to convert the *ab initio* force fiel in Cartesian coordinates to a fiel in the desired internal coordinates. The force constants for all three conformers can be obtained from the authors. The force field in internal coordinates were then assigned scaling factors. Initially, all scaling factors were

Table 1. Observed[a] infrared and Raman wavenumbers $\tilde{\nu}$ for 3-chloro-1-butene

Infrared				Raman									
$\tilde{\nu}$/cm^{-1} gas	Rel. int.	$\tilde{\nu}$/cm^{-1} soln.	Rel. int.	$\tilde{\nu}$/cm^{-1} solid	Rel. int.	$\tilde{\nu}$/cm^{-1} gas	Rel. int.	$\tilde{\nu}$/cm^{-1} liquid	Rel. int. & depol.	$\tilde{\nu}$/cm^{-1} solid	Rel. int.	ν_i[b]	Assignment Approximate description
3110 *Q*	m	3100	m, sh									ν_1''	
3102 *R*													
3097 *Q*, *C*	s	3088	m	3084	s	3098	m	3089	m	3086	s	ν_1	=CH_2 antisymmetric stretch
3091 *P*													
3085	w, sh	3075	w									ν_1'	
		3025	w			3036	sh	3026	s			ν_4'	
3027 max.	w	3017	w	3011	w	3026	vs	3014	s	3014	s, sh	ν_2	=CH stretch
		3011										ν_2'	
3002 *Q*, *C*	s			2993	s					2995	vs	ν_3	CH_3 antisymmetric stretch
2998 *Q*, *C*	vs												
2995 *Q*, *C*	vs	2990	s	2986	s	3000	vs	2989	vs	2987	vs	ν_4	=CH_2 symmetric stretch
2990 *P*													
2990 *R*													
2983 *Q*, *C*	vs	2974	s	2974	vs					2977	s	ν_5	CH_3 antisymmetric stretch
2977 *P*													
						2967	m	2960	m	2964	vs	ν_6	CH stretch
2945 *R*	s											ν_7'	
2935 *Q*	s	2927	m	2927	s	2941	vs	2930	vs	2928	vs	ν_7	CH_3 symmetric stretch
2893 *R*		2884	w										
2888, min., *B*	m	2878	w	2880	w	2890	m	2877	w	2880	w	$\nu_8 + \nu_{15}$	
2883 *P*		2865	w	2866	w								
2828 max.	vw	2823	vw							2830	vw	$\nu_8 + \nu_{16}$	
		2816	vw										
2742 max.	vw	2729	vw	2740	w	2740	w	2730	w	2728	w	$2\nu_{13}$	
1862 *R*													
1855 *Q*, *A*	m	1851	m	1880	w							$2\nu_{21}$	
1848 *P*				1875	w, sh								
										1648	m		
1650 *Q*	m	1645	m	1637	m	1651	s	1643	s	1639	vs	ν_8	C=C stretch
1461 *Q*	m											ν_{10}'	
1459 *Q*	m	1452	m	1455	m			1451	w	1460	m	ν_9	CH_3 antisymmetric deformation
				1448	m					1449	m		
1452 *Q*, *C*	s	1447	s	1446	s	1456	w	1445	w	1447	m	ν_{10}	CH_3 antisymmetric deformation
1437 *R*													
1432 *Q*													
1430 *Q*	m	1424	m	1427	s	1429	w	1424	w	1424	m	ν_{11}	=CH_2 deformation
1424 *P*													
1418 *Q*													
1416 *Q*, *C*	m	1410	m	1408	s	1417	w	1412	w	1408	m		Fermi resonance ($2\nu_{23}$)
1411 *P*													
1386 *R*													
1380 *Q*, *A*	m	1375	s	1372	vs	1380	vw	1376	vw	1375	w	ν_{12}	CH_2 symmetric deformation
1377 *P*													
1330 max.	vw	1335	vw					1328	vw			ν_{13}'	
1309 *R*													
1304 *Q*	vw	1302	w									ν_{13}''	
1300 *Q*	vw	1297	w, sh	1307	w	1306	w	1306	w	1308	s	ν_{13}	CH bend
1295 *Q*	w	1293	w									ν_{14}''	
1292 *Q*	w	1288	w									ν_{14}'	
1285 *Q*	vw	1283	vw, sh	1282	vw	1292	w	1290	w	1286	s	ν_{14}	=CH bend
1261 *R*													
1258 *Q*	m	1253	m					1253	vw			ν_{15}''	
1244 *R*				1240	w					1234	vw		
1237 *Q*, *A*	vs	1233	s	1231	vs	1238	w	1233	vvw	1228	vw	ν_{15}	CH bend
1232 *P*													
1225 *Q*	s, sh	1222	m			1228	w	1223	w			ν_{15}'	
1183 *R*													

Table 1. (*continued*)

Infrared				Raman								
$\tilde{\nu}$/cm^{-1} gas	Rel. int.	$\tilde{\nu}$/cm^{-1} soln.	Rel. int.	$\tilde{\nu}$/cm^{-1} solid	Rel. int.	$\tilde{\nu}$/cm^{-1} gas	Rel. int.	$\tilde{\nu}$/cm^{-1} liquid	Rel. int. & depol.	$\tilde{\nu}$/cm^{-1} solid	Rel. int.	ν_i[b]	Assignment Approximate description
1178 *Q, A*	m	1174	m	1175	s	1177	w	1175	w	1175	m	ν_{16}	CCC antisymmetric stretch
1176 *Q, A*	m												
1169 *P*													
1157 *Q, C*	w	1153	w					1157	vvw, sh			ν_{16}'	
1150 *P*													
1113 *Q, A*	vw	1108	w					1105	vvw, sh			ν_{18}''	
1095 *R*													
1092 *Q*	w	1090	w	1096	m	1091	w	1091	w	1096	m	ν_{17}	CH_3 rock
1086 *R*													
1082 *Q, A*	m											ν_{16}''	
1078 *Q, A*	m	1075	m					1074	w, sh			ν_{18}'	
1073 *P*													
1037 *R*													
1032 *Q*	s												
1029 *Q, A*	s	1025	vs	1018	vs	1024	w	1025	w	1018	m	ν_{18}, ν_{17}', ν_{20}''	CH_3 rock
1023 *P*													
996 *Q*	s	992	m									ν_{19}'	
993 *R*													
988 min., *B*	s	986	s	994	s	981	vw	986	vw, sh	994	w	ν_{19}	$=CH_2$ twist
985 *Q*	s											ν_{19}''	
983 *P*													
979 *Q*	s											ν_{20}''	
977 *Q*	s	976	m					976	vw, sh		ν_{17}''		
970 *Q*	m	966	m	964	s			968	w	967	w	ν_{20}	$=CH_2$ rock
932 *Q*	vs	924	vs	932	s			932	vw	936	m	ν_{21}	$=CH_2$ wag
930 *R*													
927 *Q, A*	vs											ν_{21}', ν_{21}''	
921 *P*													
872 *R*													
866 *Q, A*	m	864	m	862	s	863	w, bd	863	w	862	m	ν_{22}, ν_{22}''	CCC symmetric stretch
861 *P*													
856 *Q*	w, sh	853	w			853	vw, sh	843	vw, sh			ν_{22}'	
721 *Q*	vs	716	s									ν_{24}'	
720 *R*													
715 *Q*	vs	708	vs	710	s	713	m	707	m	710	vs	ν_{23}	CCl stretch
711 *Q*													
708 *P*													
703 *Q*	vs	699	m, sh									ν_{23}''	
638 *R*													
631 *Q*	m	625	m	623	s	629	m	624	m	624	s	ν_{24}	CH bend
628 *Q*	m					608	w					ν_{24}''	
624 *P*													
600 *Q*	w, sh	595	w			599	w	592	w			ν_{23}'	
511 *Q*	vw	507	w			508	m	508	m			ν_{25}', ν_{25}''	
464 *R*													
458 *Q, A*	w	456	m	455	m	459	m	459	m	457	s	ν_{25}	C=CC bend
451 *P*				453	w	366	vw	372	vw			ν_{26}''	
351 *R*													
344 *Q*	w							348	m			ν_{27}'	
341 *Q*	w												
335 *P*													
319 max.	w			327	s	324	w	322	vw, sh	325	w	ν_{26}, ν_{29}'	CCC bend
						317	w					ν_{28}''	
311 *R*													
305 *Q, A*	m			310	s	305	w	310	w	306	m	ν_{27}	CCl bend
302 *Q*	m			307	s							ν_{28}'	
291 *R*													
284 *Q, A*				297	s								
283 *Q, A*	vs			293	vs	283	w	289	w	295	m	ν_{28}	CCl bend
277 *P*													
247 *Q*	vw			272	m	246	vw	252	vw	277	w	ν_{29}	CH_3 torsion

(*continued overleaf*)

Table 1. (*continued*)

Infrared				Raman								
$\tilde{\nu}$/cm^{-1} gas	Rel. int.	$\tilde{\nu}$/cm^{-1} soln.	Rel. int.	$\tilde{\nu}$/cm^{-1} solid	Rel. int.	$\tilde{\nu}$/cm^{-1} gas	Rel. int.	$\tilde{\nu}$/cm^{-1} liquid	Rel. int. & depol.	$\tilde{\nu}$/cm^{-1} solid	Rel. int.	Assignment ν_i[b]	Approximate description
245 *Q*	vw											ν_{26}'	
96 *Q*										146	w		
92 *Q*	vw			126	vw	99	m	100	bd, w	137	m	ν_{30}, ν_{30}', ν_{30}''	Asymmetric torsion
90 *Q*						86	m			127	s		
				94	m								
				81	m					78	m		
										69	w		
										60	w		Lattice modes
										33	m		
										28	w		

[a] Abbreviations: s strong; m, moderate; w, weak; v, very; bd, broad; sh, shoulder; p, polarized; dp, depolarized; *A*, *B* and *C* refer to infrared band envelopes; *P*, *Q* and *R* refer to the rotational–vibrational branches, the prime indicates *gauche*-2 modes and double primes indicate *cis* modes.
[b] ν_i, ν_i' and ν_i'' refer to the HE, ME and ClE conformers, respectively.

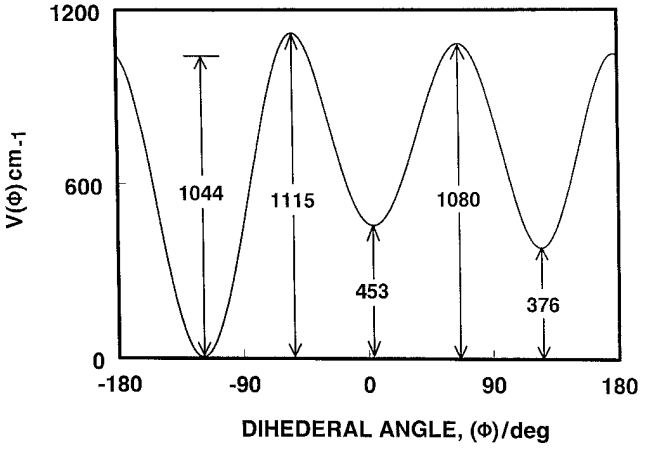

Figure 6. Potential function of the asymmetric torsion of 3-chloro-1-butene predicted from the MP2/6–31G* calculations.

kept fixe at 1.0 to reproduce the pure *ab initio* calculated vibrational wavenumbers. Subsequently, scaling factors of 0.9 for stretching and bending coordinates, 1.0 for torsional coordinates and the geometric average of scaling factors for the interaction constants were used to obtain the 'fixe scaled' force fiel and resultant wavenumbers along with the potential energy distributions (P.E.D.) which are given in Tables 5–7.

CONFORMATIONAL STABILITY

There are several conformer bands in the infrared spectra of the flui phases which disappear in the spectrum of the solid. Some of them are the A-type bands at 1157 and 1082 cm^{-1} in the spectrum of the gas, which are assigned to the CCC antisymmetric stretches of the ME and CIE conformers, respectively, as well as the bands at 1075 and 1108 cm^{-1} in the spectrum of the xenon solution assigned to the CH_3 rocks of these two forms. The corresponding fundamentals of the HE rotamer, ν_{16} and ν_{18}, are clearly seen in the infrared spectrum of the solid at 1175 and 1025 cm^{-1}, respectively.

The Raman spectra also show clear evidence for the existence of more than one conformer in the flui phases. For example, the bands located at 599 and 366 cm^{-1} in the Raman spectrum of the gas, which are assigned to modes of the ME and ClE conformers, respectively, are evident in the spectrum of the liquid but disappear in the spectrum of the crystalline solid. Similarly, the Raman bands at 508 and 348 cm^{-1} in the spectra of the liquid are not present in the spectrum of the solid. The wavenumbers in both the infrared and Raman spectra of the annealed solid are consistent with the fundamentals of the HE conformer and, therefore, it is the only form stable in this phase.

The enthalpy differences, ΔH, among the HE, ME and ClE conformers of 3-chloro-1-butene in the vapor phase can be estimated from a variable-temperature study in liquifie xenon solutions. The sample was dissolved in liquifie xenon and the spectra (Fig. 7) were recorded at different temperatures varying from -55 to $-100\,^{\circ}$C. The intensities of the well separated infrared bands at 1174, 1153 and 1108 cm^{-1} assigned (Table 1) to fundamentals of the HE, ME and ClE conformers, respectively, were measured as a function of the temperature and their ratios were determined (Table 8). By application of the van't Hoff equation, $-\ln K = (\Delta H/RT) - (\Delta S/R)$, where ΔS is the entropy change, we determined ΔH by making a plot of $-\ln K$ versus $1/T$, where $\Delta H/R$ is the slope of the line and K is the appropriate intensity ratio. It is assumed that ΔH is not a function of temperature. Using a least-squares fi and the slope of the van't Hoff plots, ΔH values of 75 ± 8 cm^{-1} (214 ± 23 cal mol^{-1}) between the HE and ME conformers and 197 ± 37 cm^{-1} (563 ± 106 cal mol^{-1}) between the HE and ClE conformers were obtained with the HE form being the most stable conformer.

VIBRATIONAL ASSIGNMENT

To aid in the vibrational assignment theoretical infrared (Fig. 5) and Raman (Fig. 8) spectra were calculated using fixe scaled wavenumbers and infrared intensities determined from the MP2/6–31G* calculation and Raman

Table 2. Structural parameters, dipole moment, total energies and rotational constants[a] for 3-chloro-1-butene

	RHF/6–31G*			MP2/6–31G*			MP2/6–311++G*			ED[b]
	HE	ME	CIE	HE	ME	CIE	HE	ME	CIE	HE
$r(C{=}C)$	1.317	1.318	1.316	1.337	1.337	1.335	1.340	1.340	1.338	1.337 (6)
$r(C_2{-}C_3)$	1.499	1.504	1.506	1.492	1.497	1.500	1.492	1.498	1.501	1.503 (4)
$r(C_3{-}C_5)$	1.522	1.519	1.526	1.519	1.515	1.523	1.520	1.516	1.524	1.522 (5)
$r(C{-}Cl)$	1.819	1.822	1.806	1.807	1.811	1.794	1.803	1.806	1.789	1.813 (4)
$r(C{-}H_6)$	1.079	1.081	1.081	1.093	1.094	1.095	1.092	1.093	1.094	1.089 (18)
$r(C{-}H_7)$	1.077	1.074	1.073	1.086	1.084	1.083	1.086	1.084	1.084	1.089 (18)
$r(C{-}H_8)$	1.075	1.075	1.075	1.084	1.085	1.084	1.084	1.085	1.084	1.089 (18)
$r(C{-}H_9)$	1.077	1.077	1.080	1.089	1.088	1.090	1.089	1.088	1.090	1.089 (18)
$r(C{-}H_{10})$	1.083	1.082	1.083	1.092	1.091	1.092	1.092	1.091	1.092	1.089 (18)
$r(C{-}H_{11})$	1.086	1.085	1.086	1.094	1.094	1.094	1.094	1.094	1.095	1.089 (18)
$r(C{-}H_{12})$	1.084	1.083	1.083	1.093	1.092	1.092	1.093	1.092	1.093	1.089 (18)
$<(C{=}CC)$	123.8	126.1	128.7	123.3	125.4	127.7	123.3	125.3	127.5	122.9 (2.1)
$<(CCC)$	112.9	116.3	111.8	112.5	115.6	111.3	112.5	115.7	111.3	112.6 (2.2)
$<(C_2C_3H_6)$	110.2	109.0	108.8	109.9	109.1	109.0	109.8	109.0	108.7	110.0 (1.3)
$<(C_5C_3H_6)$	110.5	109.8	109.5	110.5	109.9	109.5	110.6	110.1	109.5	110.0 (1.3)
$<(H_6C_3Cl)$	104.7	103.5	104.3	105.5	104.1	104.9	105.8	104.4	105.3	104.7
$<(C_2C_3Cl)$	109.2	108.3	112.9	109.2	108.2	112.8	108.8	107.8	112.9	109.9 (0.2)
$<(C_5C_3Cl)$	108.9	109.2	109.2	109.1	109.3	109.2	109.1	109.2	109.0	109.3
$<(C{=}CH_7)$	122.0	123.1	122.6	121.6	122.8	122.0	121.1	122.3	121.7	121.9
$<(C{=}CH_8)$	121.4	120.6	120.4	121.6	120.7	120.6	121.3	120.4	120.2	121.9
$<(C{=}CH_9)$	120.5	119.5	119.1	120.7	119.6	119.4	120.7	119.6	119.3	121.9
$<(C_3C_2H_9)$	115.7	114.5	112.2	116.0	115.0	113.0	116.0	115.0	113.2	115.2
$<(H_7C_1H_8)$	116.6	116.3	117.0	116.8	116.6	117.4	117.6	117.2	118.1	116.2
$<(CCH_{10})$	110.9	110.2	110.9	111.0	110.2	110.9	110.9	110.1	110.8	110.0 (1.3)
$<(CCH_{11})$	109.1	109.6	109.5	109.2	109.8	109.6	109.2	109.9	109.7	110.0 (1.3)
$<(CCH_{12})$	110.9	111.2	110.6	110.5	110.7	110.0	110.3	110.7	109.9	110.0 (1.3)
$<(H_{10}CH_{11})$	108.8	108.4	108.4	108.9	108.5	108.6	109.0	108.6	108.8	108.9
$<(H_{10}CH_{12})$	108.5	108.5	108.9	108.5	108.5	109.0	108.6	108.4	108.9	108.9
$<(H_{11}CH_{12})$	108.5	108.9	108.5	108.7	109.0	108.7	108.8	109.1	108.8	108.9
$\tau(CCCH_{10})$	178.9	179.7	183.3	179.1	179.4	182.7	178.9	179.0	182.7	180.0
$\tau(CC{=}CH_7)$	2.0	−1.3	−0.7	2.2	−0.9	−1.3	2.0	−0.8	−1.3	0.0
$\tau(CC{=}CH_8)$	180.9	178.4	182.6	181.3	178.5	181.4	180.9	178.2	181.4	180.0
$\tau(CC{=}CH_9)$	−178.7	181.0	180.4	178.5	180.7	181.0	178.7	180.7	181.1	180.0
$\tau(C{=}CCCl)$	−119.1	125.2	3.6	−119.1	124.8	3.9	−117.1	124.5	4.3	−119.4
$\lvert\mu_a\rvert$	2.032	2.162	1.377	1.969	2.100	1.304	1.810	1.972	1.184	
$\lvert\mu_b\rvert$	1.466	0.978	1.792	1.431	0.944	1.753	1.456	1.004	1.794	
$\lvert\mu_c\rvert$	0.341	0.771	0.427	0.330	0.764	0.411	0.361	0.740	0.426	
$\lvert\mu_t\rvert$	2.529	2.499	2.300	2.456	2.426	2.223	2.351	2.333	2.191	
A	5725	6458	4823	5746	6518	4821	5692	6498	4835	5737
B	2751	2685	3477	2759	2694	3523	2787	2707	3522	2724
C	2024	2078	2200	2035	2094	2225	2044	2102	2230	2015
$-(E+615)$	0.009791	0.007846	0.007222	0.68411	0.682398	0.682046	0.930539	0.928735	0.928196	
$\Delta E/cm^{-1}$	0	427	564	0	376	453	0	396	514	

[a] Bond lengths in Å, bond angles in degrees, rotational constants in MHz, energies in Hartree and dipole moments in Debye.
[b] Ref. 3.

scattering activities and depolarization values determined from the RHF/6–31G* basis set. Infrared intensities were calculated based on the dipole moment derivatives with respect to the Cartesian coordinates. The derivatives were taken from the *ab initio* calculations and transformed to normal coordinates by

$$\left(\frac{\partial \mu_u}{\partial Q_i}\right) = \sum_j \left(\frac{\partial \mu_u}{\partial X_j}\right) L_{ij}$$

where Q_i is the ith normal coordinate, X_j is the jth Cartesian displacement coordinate and L_{ij} is the transformation matrix between the Cartesian displacement coordinates and normal coordinates. The infrared intensities were then calculated by

$$I_i = \frac{N\pi}{3c^2}\left[\left(\frac{\partial \mu_x}{\partial Q_i}\right)^2 + \left(\frac{\partial \mu_y}{\partial Q_i}\right)^2 + \left(\frac{\partial \mu_z}{\partial Q_i}\right)^2\right]$$

Table 3. Potential function coefficient for asymmetric torsion of 3-chloro-1-butene and barriers to interconversion from *ab initio* MP2/6–31G* calculations

Parameter	Value	Parameter	Value
V_1/cm^{-1}	−207	V_1'/cm^{-1}	241
V_2/cm^{-1}	−94	V_2'/cm^{-1}	−225
V_3/cm^{-1}	782	V_3'/cm^{-1}	−118
V_4/cm^{-1}	−56	V_4'/cm^{-1}	13
V_5/cm^{-1}	5	V_5'/cm^{-1}	31
V_6/cm^{-1}	−13		
$\Delta H/cm^{-1}$: ME/HE	376	$\Delta H/cm^{-1}$. CIE/HE	453
CIE/ME barrier/cm^{-1}	627	Dihedral angle: HE/°	−119.1
ME/HE barrier/cm^{-1}	668	Dihedral angle: ME/°	124.8
HE/CIE barrier/cm^{-1}	1115	Dihedral angle: CIE/°	3.9

The predicted infrared spectra of the ClE, ME and HE conformers are shown in Fig. 5(C), (D) and (E), respectively, with the mixture of the two conformers shown in

Table 4. Symmetry coordinates for 3-chloro-1-butene

Description	Symmetry coordinate[a]
=CH_2 antisymmetric stretch	$S_1 = r_2 - r_1$
=CH stretch	$S_2 = P$
CH_3 antisymmetric stretch	$S_3 = 2r_3 - r_4 - r_5$
=CH_2 symmetric stretch	$S_4 = r_2 + r_1$
CH_3 antisymmetric stretch	$S_5 = r_4 - r_5$
CH stretch	$S_6 = T$
CH_3 symmetric stretch	$S_7 = r_3 + r_4 + r_5$
C=C stretch	$S_8 = Q$
CH_3 antisymmetric deformation	$S_9 = \theta_2 - \theta_3$
CH_3 antisymmetric deformation	$S_{10} = 2\theta_1 - \theta_2 - \theta_3$
=CH_2 deformation	$S_{11} = 2\alpha - \beta_1 - \beta_2$
CH_3 symmetric deformation	$S_{12} = \theta_1 + \theta_2 + \theta_3 - \zeta_1 - \zeta_2 - \zeta_3$
CH bend	$S_{13} = \eta_1 - \eta_2$
=C—H bend	$S_{14} = \phi - \mu$
CH bend	$S_{15} = 2\eta_3 - \eta_1 - \eta_2$
CCC antisymmetric stretch	$S_{16} = R - S$
CH_3 rock	$S_{17} = \zeta_2 - \zeta_3$
CH_3 rock	$S_{18} = 2\zeta_1 - \zeta_2 - \zeta_3$
=CH_2 twist	$S_{19} = \tau_1$
=CH_2 rock	$S_{20} = \beta_2 - \beta_1$
=CH_2 wag	$S_{21} = \gamma$
CCC symmetric stretch	$S_{22} = R + S$
CCl stretch	$S_{23} = Y$
=CH bend	$S_{24} = \sigma$
C=C—C bend	$S_{25} = 2\pi - \phi - \mu$
CCC bend	$S_{26} = \nu_3$
CCl bend	$S_{27} = \nu_1 + \nu_2$
CCl bend	$S_{28} = \nu_1 - \nu_2$
CH_3 torsion	$S_{29} = \tau_2$
Asymmetric torsion	$S_{30} = \tau_3$

[a] Not normalized.

Fig. 5(B) using the experimentally determined ΔH values from the liquifie xenon. The calculated spectrum is in reasonably good agreement with the mid-infrared spectrum of the sample dissolved in liquid xenon [Fig. 5(A)]. Only minor discrepancies are encountered between the observed and calculated spectra. These are primarily due to wavenumber inconsistencies such as the prediction of nearly coincident CH bending modes for the HE and ME conformers as opposed to the observed two separate bands for these fundamentals at 1233 and 1222 cm^{-1}.

The evaluation of the Raman activity by using the analytical gradient methods has been developed.[10,11] The activity S_j can be expressed as

$$S_j = g_j(45\alpha_j^2 + 7\beta_j^2)$$

where g_j is the degeneracy of the vibrational mode j, α_j is the derivative of the isotropic polarizability and β_j is that of the anisotropic polarizability. The Raman scattering cross-sections, $\partial\sigma_j/\partial\Omega$, which are proportional to the Raman intensities, can be calculated from the scattering activities and the predicted wavenumbers for each normal mode using the relationship[12,13]

$$\frac{\partial\sigma_j}{\partial\Omega} = \left(\frac{2^4\pi^4}{45}\right)\left(\frac{(\nu_0 - \nu_j)^4}{1 - \exp\left[\frac{-hc\nu_j}{kT}\right]}\right)\left(\frac{h}{8\pi^2 c\nu_j}\right)S_j$$

where ν_0 is the exciting wavenumber, ν_j is the vibrational wavenumber of the jth normal mode and S_j is the corresponding Raman scattering activity. To obtain the polarized Raman scattering cross-sections, the polarizabilities are incorporated into S_j by $S_j[(1 - \rho_j)/(1 + \rho_j)]$, where ρ_j is the depolarization ratio of the jth normal mode. The Raman scattering cross-sections and calculated f xed scaled wavenumbers are used together with a Lorentzian function to obtain the calculated spectra.

The resulting spectra are shown in Fig. 8(C), (D) and (E) for the pure ClE, ME and HE conformers, respectively, with the spectrum of the mixture shown in Fig. 8(B). For comparison, the Raman spectrum of the liquid is also shown in Fig. 8(A). The resemblance between the observed and calculated Raman spectra, however, is not as good as that of the corresponding infrared spectra. Various differences are readily seen with some of them due to poor wavenumber predictions as mentioned earlier. Others are due to poor Raman intensity predictions such as the very high intensity of the CCl bending fundamental at 283 cm^{-1}. It is not clear whether the intensities of the fundamentals at 592 and 508 cm^{-1}, which belong to the less stable ME and ClE conformers, are predicted too strong because of underestimated ΔH values or because of too high Raman activities predicted by the RHF/6–31G* basis set. Nevertheless, these spectra were useful for making the vibrational assignments for the individual conformers.

The vibrational assignment of the mid-infrared and Raman spectra of 3-chloro-1-butene has been proposed by Schei and Klaeboe.[2] Based on our normal coordinate calculations, we suggested the assignment of the fundamentals observed in the mid-infrared spectrum of the sample dissolved in liquid xenon as well (Table 1). We shall discuss here only the assignments that are at variance with the previous vibrational assignment.[2]

First, the band at 2880 cm^{-1}, which was previously[2] assigned to the CH_3 symmetric stretch, ν_7, is now attributed to a combination band. Thus, four of the seven carbon–hydrogen stretching fundamentals, ν_4–ν_7, are shifted to higher wavenumbers as ν_7 is assigned to the very strong band at 2930 cm^{-1} in the Raman spectrum of the liquid. Another discrepancy between the two studies arises from the assignment of the band at 1416 cm^{-1} in the infrared spectrum of the gas. This band is probably part of a Fermi resonance doublet of the overtone of the CCl stretch with the =CH_2 deformation. Alternatively, the previous authors[2] assigned the band to the =CH_2 deformation, ν_{11}, having the two CH_3 antisymmetric deformations assigned at 1452 and 1430 cm^{-1} and the band at 1459 cm^{-1} assigned to the high-energy conformers. The latter band, however, is still present in the Raman spectrum of the solid and, therefore, we assigned it to one of the CH_3 antisymmetric deformations of the stable conformer.

Some additional fundamentals of the high-energy conformers were observed in the spectra of the sample dissolved in liquid xenon. For example, the band at 1302 cm^{-1} is assigned to the CH bend of the CIE conformer, whereas the bands at 1293 and 1288 cm^{-1} are attributed to the =CH bends of the CIE and ME rotamers. In addition, the =CH_2 twists of the ME and CIE conformers are observed at 992 and 983 cm^{-1}, respectively, whereas the band at 669 cm^{-1} is due to the CCl stretch of

Table 5. Comparison of observed and calculated wavenumbers ($\tilde{\nu}$) for HE 3-chloro-1-butene

Species	Vib. No.	Fundamental	*Ab initio*[a] $\tilde{\nu}$/cm^{-1}	Fixed scaled[b] $\tilde{\nu}$/cm^{-1}	IR int.[c]	Raman act.[d]	DP ratio	Obs.[e] $\tilde{\nu}$/cm^{-1}	P.E.D.
A	ν_1	=CH_2 antisymmetric stretch	3310	3141	9.1	75.4	0.61	3088	$98S_1$
	ν_2	=CH stretch	3224	3058	3.5	88.3	0.29	3017	$67S_2$, $28S_4$
	ν_3	CH_3 antisymmetric stretch	3216	3051	12.4	70.6	0.12	3011	$77S_3$, $17S_5$
	ν_4	=CH_2 symmetric stretch	3212	3048	5.7	30.5	0.13	2990	$64S_4$, $31S_2$
	ν_5	CH_3 antisymmetric stretch	3205	3040	11.6	85.3	0.74	2974	$80S_5$, $18S_3$
	ν_6	CH stretch	3156	2994	5.9	83.4	0.68	2967*	$97S_6$
	ν_7	CH_3 symmetric stretch	3111	2952	10.4	107.8	0.02	2927	$99S_7$
	ν_8	C=C stretch	1731	1642	0.7	50.5	0.19	1645	$67S_8$, $16S_{11}$
	ν_9	CH_3 antisymmetric deformation	1557	1477	3.5	16.6	0.75	1452	$74S_9$, $18S_{10}$
	ν_{10}	CH_3 antisymmetric deformation	1549	1469	7.1	16.2	0.73	1447	$72S_{10}$, $18S_9$
	ν_{11}	=CH_2 deformation	1503	1426	8.3	14.0	0.31	1424	$73S_{11}$
	ν_{12}	CH_3 symmetric deformation	1467	1392	7.3	1.9	0.72	1375	$96S_{12}$
	ν_{13}	CH bend	1372	1302	2.0	17.8	0.56	1297	$62S_{13}$
	ν_{14}	=C—H bend	1348	1279	4.7	15.1	0.41	1283	$51S_{14}$, $17S_{15}$, $13S_8$
	ν_{15}	CH bend	1323	1255	23.9	6.3	0.73	1233	$67S_{15}$, $11S_{14}$
	ν_{16}	CCC antisymmetric stretch	1239	1175	8.3	6.8	0.71	1174	$20S_{16}$, $17S_{18}$, $13S_{20}$, $13S_{22}$
	ν_{17}	CH_3 rock	1154	1095	1.7	5.8	0.40	1090	$29S_{17}$, $36S_{16}$, $12S_{22}$
	ν_{18}	CH_3 rock	1085	1030	32.7	7.5	0.74	1025	$37S_{18}$, $14S_{17}$, $13S_{16}$
	ν_{19}	=CH_2 twist	1033	981	19.3	0.5	0.74	988*	$59S_{19}$, $35S_{24}$
	ν_{20}	=CH_2 rock	1011	960	3.6	1.1	0.75	966	$30S_{20}$, $26S_{17}$, $13S_{13}$
	ν_{21}	=CH_2 wag	948	899	36.0	2.4	0.71	931*	$98S_{21}$
	ν_{22}	CCC symmetric stretch	911	864	8.4	7.6	0.72	864	$47S_{22}$, $19S_{18}$, $19S_{20}$
	ν_{23}	CCl stretch	751	713	35.0	18.3	0.42	708	$29S_{23}$, $18S_{24}$, $15S_{27}$, $13S_{19}$
	ν_{24}	=CH bend	667	634	5.7	10.5	0.37	625	$24S_{24}$, $30S_{23}$, $19S_{19}$
	ν_{25}	C=C—C bend	473	449	3.6	10.1	0.13	456	$22S_{25}$, $28S_{23}$, $15S_{26}$, $14S_{22}$, $12S_{27}$
	ν_{26},	CCC bend	333	319	1.0	0.8	0.64	319*	$46S_{26}$, $19S_{29}$, $15S_{25}$, $12S_{28}$
	ν_{27}	CCl bend	313	298	1.0	2.5	0.69	305*	$43S_{27}$, $26S_{25}$, $22S_{28}$
	ν_{28}	CCl bend	294	281	2.4	7.1	0.71	283*	$40S_{28}$, $14S_{27}$, $13S_{26}$, $10S_{29}$
	ν_{29}	CH_3 torsion	271	267	0.8	0.2	0.72	245*	$68S_{29}$, $12S_{28}$, $10S_{25}$
	ν_{30}	Asymmetric torsion	100	99	0.2	8.7	0.75	92*	$85S_{30}$

[a] Calculated using the MP2/6–31G* basis set.
[b] Scaled *ab initio* calculations with factors of 0.9 for stretches and bends and 1.0 for torisions.
[c] Calculated intensities in km mol^{-1} using the MP2/6–31G* basis set.
[d] Calculated Raman activities in Å^4 u^{-1} using the RHF/3–21G* basis set.
[e] Wavenumbers are taken from the infrared spectrum of the sample dissolved in liquid xenon, except those labeled with an asterisk, which are taken from the infrared spectrum of the gas or the Raman spectrum of the gas and liquid.

the CIE form. The above-cited bands have no analogues in the spectra of the crystalline solid.

The methyl torsional mode produces very weak bands at 246, 252 and 277 cm^{-1} in the Raman spectra of the gas, liquid and solid, respectively, and also the pair of *Q*-branches at 247/245 cm^{-1} in the far-infrared spectrum of the gas. Finally, the medium-intensity band observed at 99 cm^{-1} in the Raman spectrum of the gas must result from the asymmetric torsional mode. This choice is consistent with the study of 3-methyl-1-butene.[14] The asymmetric torsion is also observed in the far-infrared spectrum of the gas with a fundamental at 92 cm^{-1} and possible fundamentals for the high-energy conformers at 96 and 90 cm^{-1}.

DISCUSSION

The present study of 3-chloro-1-butene is consistent with the previous vibrational[2] and electron diffraction[3] studies in the conclusion that the most stable conformer of the

Table 6. Comparison of observed and calculated wavenumbers ($\tilde{\nu}$) for ME 3-chloro-1-butene

Species	Vib. No.	Fundamental	*Ab initio*[a] $\tilde{\nu}$/cm^{-1}	Fixed scaled[b] $\tilde{\nu}$/cm^{-1}	IR int.[c]	Raman act.[d]	DP ratio	Obs.[e] $\tilde{\nu}$/cm^{-1}	P.E.D.
A	ν_1	=CH_2 antisymmetric stretch	3319	3148	8.2	61.3	0.68	3088	$99S_1$
	ν_2	=CH stretch	3221	3056	5.1	136.1	0.18		$55S_2$, $40S_4$
	ν_3	CH_3 antisymmetric stretch	3224	3059	9.9	40.5	0.30		$70S_3$, $24S_5$
	ν_4	=CH_2 symmetric stretch	3234	3068	4.1	45.2	0.50	3075	$59S_4$, $40S_2$
	ν_5	CH_3 antisymmetric stretch	3210	3045	10.7	52.3	0.73		$73S_5$, $26S_3$
	ν_6	CH stretch	3143	2982	8.8	122.3	0.43		$99S_6$
	ν_7	CH_3 symmetric stretch	3118	2958	8.3	94.7	0.04	2927	$99S_7$
	ν_8	C=C stretch	1731	1642	1.2	41.8	0.20	1645	$67S_8$, $16S_{11}$
	ν_9	CH_3 antisymmetric deformation	1555	1475	7.1	7.9	0.65	1452	$58S_9$, $33S_{10}$
	ν_{10}	CH_3 antisymmetric deformation	1561	1481	3.7	14.9	0.70		$55S_{10}$, $36S_9$
	ν_{11}	=CH_2 deformation	1496	1420	9.7	20.0	0.51		$68S_{11}$
	ν_{12}	CH_3 symmetric deformation	1467	1392	8.8	5.8	0.55	1375	$82S_{12}$
	ν_{13}	CH bend	1413	1340	1.8	3.6	0.60	1335	$60S_{13}$, $12S_{16}$
	ν_{14}	=C—H bend	1360	1290	0.8	15.3	0.34	1288	$60S_{14}$, $15S_8$, $11S_{20}$
	ν_{15}	CH bend	1324	1257	34.1	22.8	0.60	1222	$87S_{15}$
	ν_{16}	CCC antisymmetric stretch	1216	1154	3.8	1.9	0.66	1153	$35S_{16}$, $14S_{20}$, $13S_{17}$
	ν_{17}	CH_3 rock	1074	1019	7.8	3.6	0.75	1025	$39S_{17}$, $13S_{13}$, $11S_{20}$
	ν_{18}	CH_3 rock	1133	1075	13.8	3.3	0.58	1075	$50S_{18}$
	ν_{19}	=CH_2 twist	1047	994	13.6	1.3	0.47	992	$60S_{19}$, $33S_{24}$
	ν_{20}	=CH_2 rock	1029	976	12.0	1.7	0.75	976	$33S_{20}$, $21S_{16}$, $15S_{22}$, $10S_{17}$
	ν_{21}	=CH_2 wag	945	896	34.9	5.2	0.73	924	$99S_{21}$
	ν_{22}	CCC symmetric stretch	899	853	7.9	7.3	0.70	853	$57S_{22}$, $16S_{18}$, $10S_{20}$
	ν_{23}	CCl stretch	629	597	8.8	19.8	0.51	595	$39S_{23}$, $12S_{24}$, $11S_{25}$, $10S_{19}$, $10S_{22}$
	ν_{24}	=CH bend	760	721	28.9	14.2	0.23	716	$24S_{24}$, $25S_{25}$, $18S_{27}$, $18S_{19}$, $10S_{17}$
	ν_{25}	C=C—C bend	526	499	0.8	7.7	0.36	507	$31S_{25}$, $22S_{26}$, $12S_{23}$
	ν_{26}	CCC bend	283	269	2.2	4.5	0.35	245*	$27S_{26}$, $33S_{28}$, $22S_{25}$
	ν_{27}	CCl bend	354	337	2.7	3.5	0.61	344*	$55S_{27}$, $12S_{23}$, $12S_{28}$
	ν_{28}	CCl bend	306	300	0.4	1.0	0.75	301*	$29S_{28}$, $46S_{29}$, $13S_{26}$
	ν_{29}	CH_3 torsion	333	322	0.6	2.3	0.75	319*	$46S_{29}$, $16S_{26}$, $14S_{28}$, $13S_{25}$
	ν_{30}	Asymmetric torsion	104	104	0.3	7.3	0.75	96*	$88S_{30}$

[a] Calculated using the MP2/6–31G* basis set.
[b] Scaled *ab initio* calculations with factors of 0.9 for stretches and bends and 1.0 for torsions.
[c] Calculated intensities in km mol^{-1} using the MP2/6–31G* basis set.
[d] Calculated Raman activities in Å^4 u^{-1} using the RHF/3–21G* basis set.
[e] Wavenumbers are taken from the infrared spectrum of the sample dissolved in liquid xenon, except those labeled with an asterisk, which are taken from the infrared spectrum of the gas or the Raman spectrum of the gas and liquid.

molecule is the HE form. However, it differs from these earlier studies in the stability of the other two conformers. It is clearly shown by both the *ab initio* calculations and the measurements in liquid xenon that the ME conformer is the second most stable form, which is at variance with the electron diffraction result,[3] where it was concluded that the CIE form is the second most stable rotamer. In addition, definit evidence was found in the vibrational spectrum for the existence of the third conformer (CIE), which was not the conclusion in the previous vibrational investigation.[2]

The enthalpy differences, ΔH, obtained from the variable-temperature study in liquid xenon are consistent with the stability order of the conformers obtained from the *ab initio* calculations. However, in all cases (Table 2) the energy differences are much too high compared with the experimental values of 75±8 and 197±37 cm^{-1} and do not seem to improve upon increasing the size of the basis set. However, it is expected that these enthalpy values from the xenon solution should not differ significantl from those of the gas since the dipole moments and molecular sizes of the three conformers are very similar.[15–19]

Table 7. Comparison of observed and calculated wavenumbers ($\tilde{\nu}$) for CIE 3-chloro-1-butene

Species	Vib. No.	Fundamental	*Ab initio*[a] $\tilde{\nu}$/cm^{-1}	Fixed scaled[b] $\tilde{\nu}$/cm^{-1}	IR int.[c]	Raman act.[d]	DP ratio	Obs.[e] $\tilde{\nu}$/cm^{-1}	P.E.D.
A	ν_1	=CH_2 antisymmetric stretch	3327	3157	4.8	47.8	0.73	3092	$99S_1$
	ν_2	=CH stretch	3198	3034	3.3	132.4	0.14		$85S_2$
	ν_3	CH_3 antisymmetric stretch	3223	3057	11.8	73.0	0.43		$69S_3$, $30S_5$
	ν_4	=CH_2 symmetric stretch	3233	3068	3.9	59.3	0.64	3075	$94S_4$
	ν_5	CH_3 antisymmetric stretch	3204	3040	17.9	49.6	0.75		$61S_5$, $28S_3$, $10S_2$
	ν_6	CH stretch	3136	2975	9.2	132.9	0.41		$99S_6$
	ν_7	CH_3 symmetric stretch	3112	2953	12.7	103.2	0.03	2927	$98S_7$
	ν_8	C=C stretch	1737	1648	3.9	32.2	0.20	1645	$69S_8$, $14S_{11}$
	ν_9	CH_3 antisymmetric deformation	1558	1478	4.6	13.9	0.74	1452	$78S_9$, $15S_{10}$
	ν_{10}	CH_3 antisymmetric deformation	1550	1470	4.8	19.1	0.74	1447	$76S_{10}$, $15S_9$
	ν_{11}	=CH_2 deformation	1490	1413	6.1	11.2	0.44		$79S_{11}$
	ν_{12}	CH_3 symmetric deformation	1467	1391	7.2	2.5	0.66	1375	$96S_{12}$
	ν_{13}	CH bend	1375	1305	3.1	3.8	0.73	1302	$71S_{13}$
	ν_{14}	=C—H bend	1363	1293	17.1	16.7	0.36	1297	$40S_{14}$, $39S_{15}$
	ν_{15}	CH bend	1340	1272	9.4	11.8	0.71	1253	$41S_{15}$, $28S_{14}$, $10S_{20}$
	ν_{16}	CCC antisymmetric stretch	1145	1086	4.0	1.9	0.75	1082*	$25S_{16}$, $22S_{17}$, $19S_{22}$
	ν_{17}	CH_3 rock	1025	972	12.8	6.8	0.43	976	$23S_{17}$, $24S_{16}$, $23S_{19}$
	ν_{18}	CH_3 rock	1167	1107	10.1	2.6	0.62	1108	$22S_{18}$, $13S_{15}$, $12S_{16}$, $10S_{17}$
	ν_{19}	=CH_2 twist	1032	980	16.2	1.8	0.75	985*	$42S_{19}$, $23S_{24}$, $13S_{17}$
	ν_{20}	=CH_2 rock	1087	1032	5.2	1.1	0.75	1025	$42S_{20}$, $24S_{18}$
	ν_{21}	=CH_2 wag	944	896	34.0	4.7	0.75	924	$98S_{21}$
	ν_{22}	CCC symmetric stretch	908	862	8.8	8.6	0.65	864	$39S_{22}$, $19S_{18}$, $17S_{20}$, $11S_{23}$
	ν_{23}	CCl stretch	736	698	11.6	9.7	0.53	699	$28S_{23}$, $16S_{24}$, $16S_{27}$, $10S_{19}$, $10S_{17}$
	ν_{24}	=CH bend	657	623	13.3	15.0	0.23	625	$26S_{24}$, $23S_{23}$, $19S_{22}$, $16S_{19}$
	ν_{25}	C=C—C bend	526	499	2.9	6.3	0.60	507	$44S_{25}$, $27S_{23}$
	ν_{26}	CCC bend	378	359	0.8	2.8	0.48	366*	$35S_{26}$, $20S_{27}$, $13S_{28}$
	ν_{27}	CCl bend	258	246	0.6	1.9	0.74		$23S_{27}$, $37S_{28}$, $32S_{25}$
	ν_{28}	CCl bend	339	324	0.8	0.4	0.72		$32S_{28}$, $27S_{26}$, $15S_{27}$, $13S_{29}$
	ν_{29}	CH_3 torsion	278	276	0.2	2.5	0.63		$83S_{29}$
	ν_{30}	Asymmetric torsion	96	96	0.3	7.3	0.75	90*	$90S_{30}$

[a] Calculated using the MP2/6–31 G* basis set.
[b] Scaled *ab initio* calculations with factors of 0.9 for stretches and bends and 1.0 for torsions.
[c] Calculated intensities in km mol^{-1} using the MP2/6–31 G* basis set.
[d] Calculated Raman activities in Å^4 u^{-1} using the RHF/3–21 G* basis set.
[e] Wavenumbers are taken from the infrared spectrum of the sample dissolved in liquid xenon, except those labeled with an asterisk, which are taken from the infrared spectrum of the gas or the Raman spectrum of the gas and liquid.

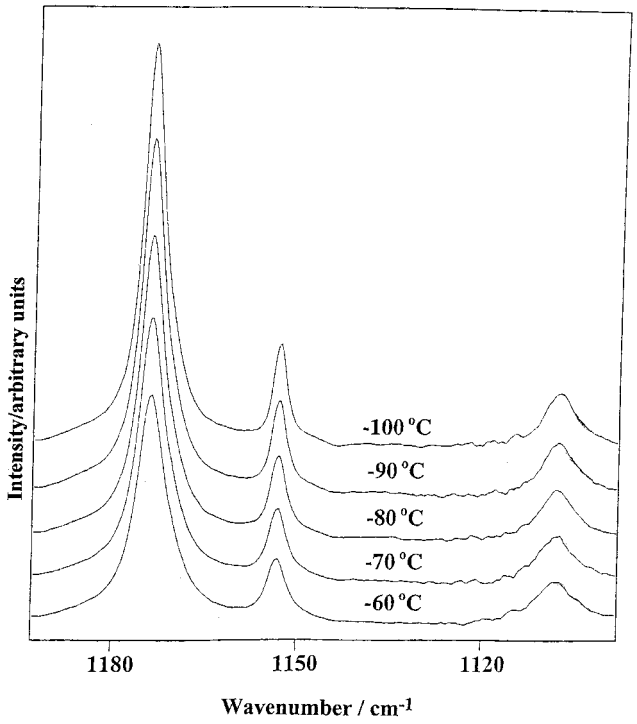

Figure 7. Temperature-dependent infrared spectrum (1190–1100 cm^{-1}) of 3-chloro-1-butene.

Table 8. Temperature and intensity ratios for the conformational study of 3-chloro-1-butene in liquid xenon

T/°C	T/K	1000/ T/K^{-1}	$I_{1153(ME)}/I_{1174(HE)}$	−LnK	$I_{1108(CIE)}/I_{1174(HE)}$	−LnK
−55	218	4.587	0.147	1.914	0.209	1.565
−60	213	4.695	0.147	1.918	—	—
−65	208	4.808	—	—	0.166	1.795
−70	203	4.926	0.145	1.934	0.181	1.707
−75	198	5.051	0.140	1.964	0.161	1.827
−80	193	5.181	0.138	1.982	—	—
−85	188	5.319	0.135	2.004	0.162	1.820
−90	183	5.464	0.134	2.010	0.146	1.924
−95	178	5.618	0.130	2.039	0.146	1.923
−100	173	5.780	0.132	2.023	0.141	1.959
ΔH/cm^{-1}				75 ± 8		197 ± 37

From the calculated potential function of the asymmetric rotor (Fig. 6), it is clear that although the energies of the conformers are different, the heights of the barriers to rotation are almost the same at about 1100 cm^{-1}. It was not possible to derive a potential function based on the experimental data since the three far-infrared transitions observed in the spectrum of the gas do not provide enough information to obtain a reasonable fi for the potential coefficients In addition, two of the three far-infrared bands may simply be due to 'hot' transitions of one of the conformers rather than fundamentals.

In the far-infrared spectra of gaseous 3-chloro-1-butene two transitions were observed in the region expected for the methyl torsion. The *ab initio* calculations predict the methyl torsions for the HE and ME forms to be at 267 and 322 cm^{-1}, respectively, with similar predicted intensities. Therefore, the bands observed at 245 and 319 cm^{-1} were assigned to the methyl torsional fundamental of

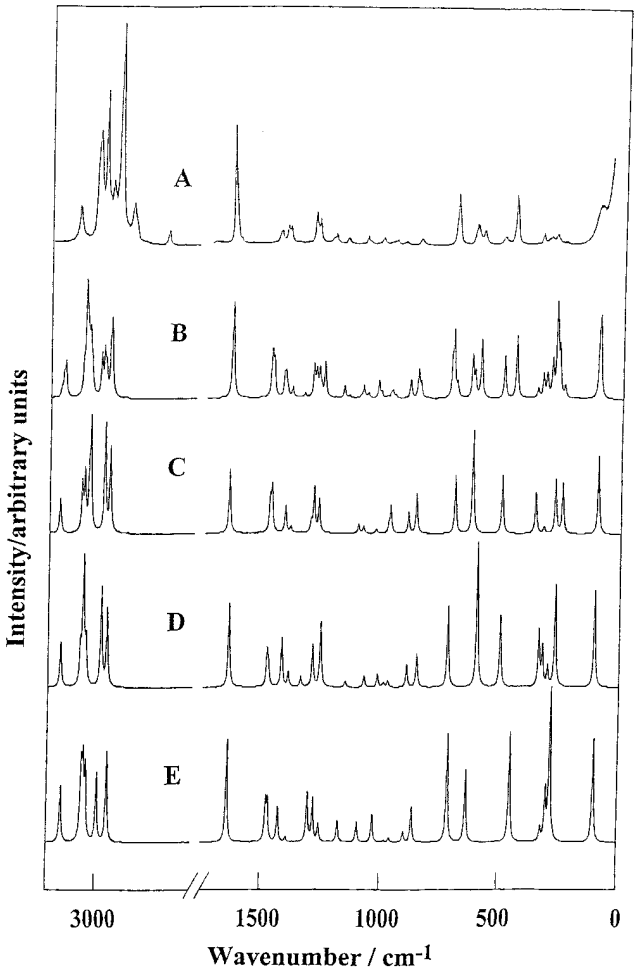

Figure 8. Raman spectra of 3-chloro-1-butene: (A) spectrum of the liquid; (B) calculated spectrum of the mixture of all three conformers; (C) calculated spectrum of the CIE conformer; (D) calculated spectrum of the ME conformer; (E) calculated spectrum of the HE conformer.

the HE and ME conformers, respectively. Utilizing the r_0 adjusted parameters, the values for the kinetic energy constants $F = h^2/8\pi^2 I_r$ (I_r is the reduced moment of inertia) were obtained for the HE ($F = 5.3982$ cm^{-1}) and ME ($F = 5.4030$ cm^{-1}) conformers. With these torsional wavenumbers and F values, the barriers to internal rotation of the methyl group were calculated and found to be 1389 and 2262 cm^{-1} for the HE and ME rotamers, respectively. These values are about 7–74% higher than corresponding barriers for 1-chloroethane.[20] It is obvious that the allyl group, which is a bulky electron-rich group, increases the value of the methyl barrier for the HE conformer. However, for the ME conformer, for which a much higher methyl barrier was calculated, it is probable that this result is due to the extensive mixing of the methyl torsion with other modes.

The structural parameters obtained from the MP2/6–31G* calculation are not significantl different from those obtained from the MP2/6–311++G** calculation. At the MP2/6–31G* level, the C=CC bond angles of the ME and CIE conformers are 2.1 and 4.4° larger, respectively, than that of the HE conformer. This could be explained with the increasingly stronger steric interaction between the $=CH_2$ fragment and the H, CH_3 and Cl substituents. The bond, which eclipses the double bond

in any particular conformation, is shorter than the same bond in the other two conformations. This is coupled with the opening of the C_2C_3H (by ~1°), CCC (by ~4°) and CCCl (by ~4°) angles for the HE, ME and CIE conformers, respectively. A comparison of the structural parameters of 3-chloro-1-butene and those of 3-methyl-1-butene[14] obtained with the MP2/6–31G* basis set shown a great deal of similarity between the HE conformers of the two molecules with the exception of the parameters associated with the substitutuent. The bond distances are within 0.01 Å and the angles within 2°. The electron diffraction (ED) geometric parameters listed in Table 2 were determined[3] only for the predominant HE conformer, and they are in excellent agreement with our results from the MP2 level of calculations. This suggests that for the other two less stable conformers the geometry should also be predicted reasonably well at the MP2 level of the *ab initio* calculations.

The force constants for the HE conformer of 3-chloro-1-butene as compared with those for the ME and CIE conformers are fairly similar, except for three. The force constant for the CCC bend of the ME conformer is 0.909 mdyn $Å^{-1}$ and is 32% larger than that of the HE conformer (0.687 mdyn $Å^{-1}$). The force constants for the CCl stretch and C=CC bend of the CIE conformer are 3.116 and 1.104 mdyn $Å^{-1}$ and are 57% (2.947 mdyn $Å^{-1}$) and 43% (0.770 mdyn $Å^{-1}$) larger than those of the HE conformer. These differences provide an explanation why several of the normal modes for the different conformers have significantl different wavenumbers.

It would be of interest to have the electron diffraction data reinterpreted using the ME conformer as the second most abundant form in the vapor state and the predicted difference of the heavy atom parameters for the three rotamers. The current conformational data indicate that there is approximately 48% HE form, 33% ME form and 19% CIE form in the gas phase at ambient temperature. Using these approximate percentages along with holding the structural parameter differences to the values obtained from the *ab initio* calculations for the three rotamers should enhance significantl the electron diffraction analysis.

Acknowledgment

J.R.D. acknowledges partial support of these studies by the University of Missouri–Kansas City Faculty Research Grant program.

REFERENCES

1. Som JN, Kastha GS. *Indian J. Phys. B* 1977; **51**: 77.
2. Schei SH, Klaeboe P. *Acta Chem. Scand., Sev. A* 1983; **37**: 315.
3. Schei SH. *J. Mol. Struct.* 1984; **118**: 319.
4. Stavnebrekk PJ, Stølevik R. *J. Mol. Struct.* 1987; **159**: 153.
5. Frisch MJ, Trucks GW, Schlegel HB, Gill PMW, Johnson BG, Robb MA, Cheeseman JR, Keith TA, Petersson GA, Montgomery JA, Raghavachari K, Al-Laham MA, Zakrzewski VG, Ortiz JV, Foresman JB, Cioslowski J, Stefanov BB, Nanayakkara A, Challacombe M, Peng CY, Ayala PY, Chen W, Wong MW, Andres JL, Replogle ES, Gomperts R, Martin RL, Fox DJ, Binkley JS, Defrees DJ, Baker J, Stewart JP, Head-Gordon M, Gonzalez C, Pople JA. *Gaussian 94 (Revision B. 3)*. Gaussian: Pittsburgh, PA, 1995.
6. Pulay P. *Mol. Phys.* 1969; **17**: 197.
7. Möller C, Plesset MS. *Phys. Rev.* 1934; **46**: 618.
8. Wilson EB, Decius JC, Cross PC. *Molecular Vibrations*. McGraw-Hill: New York, NY, 1955; republished by Dover, New York, 1980.
9. Schachtschneider JH. *Vibrational Analysis of Polyatomic Molecules, Parts V and VI*. Technical Report Nos 231 and 57, Shell Development, Houston, TX, 1964 and 1965.
10. Amos RD. *Chem. Phys. Lett.* 1986; **124**: 376.
11. Polavarapu PL. *J. Phys. Chem.* 1990; **94**: 8106.
12. Chantry GW. In *The Raman Effect*, vol. 1. Anderson A (ed). Marcel Dekker: New York, 1971; Chapt. 2.
13. Zaripov NM. *Zh. Strukt. Khim.* 1982; **23**: 142.
14. Durig JR, Tang Q, Little TS. *J. Raman Spectrosc.* 1993; **24**: 555.
15. Herrebout WA, van der Veken BJ. *J. Phys. Chem.* 1996; **100**: 9671.
16. Herrebout WA, van der Veken BJ, Wang A, Durig JR. *J. Phys. Chem.* 1995; **99**: 578.
17. Bulanin MO. *J. Mol. Struct.* 1995; **347**: 73.
18. van der Veken BJ, DeMunck FR. *J. Chem. Phys.* 1992; **97**: 3060.
19. Bulanin MO. *J. Mol. Struct.* 1973; **19**: 59.
20. Durig JR, Bucy WE, Carreira LA, Wurrey CJ. *J. Chem. Phys.* 1974; **60**: 1754.

